CHEMISTRY

Near-equilibrium growth from borophene edges on silver

Zhuhua Zhang[1,2]*, Andrew J. Mannix[3,4], Xiaolong Liu[5], Zhili Hu[1,2], Nathan P. Guisinger[3], Mark C. Hersam[4,5,6]*, Boris I. Yakobson[2]*

Two-dimensional boron, borophene, was realized in recent experiments but still lacks an adequate growth theory for guiding its controlled synthesis. Combining ab initio calculations and experimental characterization, we study edges and growth kinetics of borophene on Ag(111). In equilibrium, the borophene edges are distinctly reconstructed with exceptionally low energies, in contrast to those of other two-dimensional materials. Away from equilibrium, sequential docking of boron feeding species to the reconstructed edges tends to extend the given lattice out of numerous polymorphic structures. Furthermore, each edge can grow via multiple energy pathways of atomic row assembly due to variable boron-boron coordination. These pathways reveal different degrees of anisotropic growth kinetics, shaping borophene into diverse elongated hexagonal islands in agreement with experimental observations in terms of morphology as well as edge orientation and periodicity. These results further suggest that ultrathin borophene ribbons can be grown at low temperature and low boron chemical potential.

INTRODUCTION

Borophene, a two-dimensional (2D) boron analog to graphene, is presently attracting interest due to its distinct structural, electronic, and optical properties for many potential applications (*1*–*4*). Early theories suggested that borophene is a network of hollow hexagons (HHs) in an otherwise triangular boron lattice (*5*–*8*), a characteristic that is first confirmed experimentally in large-sized planar boron clusters (*9*, *10*). A mixture of HHs in a triangular lattice effectively compensates for the electronic deficiency of boron (*11*) and results in stabilization of borophene. However, borophene is polymorphic because of numerous possible arrangements of HHs in the triangular lattice (*12*, *13*). The HH arrangements can be mediated by metal substrate (*14*, *15*) and carrier density (*16*), such that borophene is a 2D material that does not have its own fixed lattice structure but depends on external physical conditions. Some borophene phases have been predicted to exhibit phonon-mediated superconductivity (*17*, *18*) as well as Dirac fermions (*19*, *20*) and visible range plasmonics (*21*). Recently, theoretical predictions of borophene (*14*, *15*) were confirmed (*22*, *23*) by its experimental synthesis on Ag(111). More borophene phases (*24*–*27*) and nanostructures (*28*, *29*) were synthesized subsequently on Ag(110), Al(111), and Cu(111) substrates, but to date, these efforts have required molecular beam epitaxy, which is cumbersome and challenging to scale. Consequently, further fundamental and applied studies of borophene growth are needed to develop improved synthesis methods that can achieve large-scale, high-quality samples.

Extensive theoretical studies have been devoted to the growth mechanisms of nearly isotropic 2D materials including graphene (*30*, *31*), hexagonal boron nitride (h-BN) (*32*), and transition metal dichalcogenides (*33*). A general picture is that feeding species land on the substrate and diffuse toward edges to nucleate a new atomic row, forming kinks that move via sequential addition of atoms. Such a nucleation–kink flow scenario has explained different experimental shapes for these 2D materials on growth substrates. In contrast, borophene is expressly anisotropic with a richer variety of edges, along which the growth kinetics are likely to be more complicated because of the multicenter characteristics of boron-boron bonding (*34*). In particular, feeding units of boron have many more possibilities of being organized during the edge growth in view of the polymorphism of borophene. This feature elicits a compelling question as to whether boron growth can proceed or be steered to form a given phase. These issues and new features underscore the importance of advancing the growth theory for anisotropic 2D materials of which borophene is the prototypical example.

Here, we report an atomistic growth mechanism for borophene by combining crystal growth theory with detailed first-principles calculations. First, the borophene edges are identified to be notably reconstructed on Ag(111), with the periodicities of zigzag edges doubled from the intrinsic lattice and edge energies much lower than those of graphene. The growth kinetics are then explored by extending our "nanoreactor" (*30*) model to the reconstructed edges, at which sequential docking of boron atoms not only drives the edge growth but also seamlessly extends the lattice with no change in its HH network. In contrast to graphene and h-BN, the edge growth can proceed via multiple energy pathways (EPs) with close barriers due to variable boron coordination. All EPs reveal a strong anisotropy of growth kinetics, which yields boron islands as greatly elongated hexagons with varied aspect ratios that agree well with experimental observations in terms of morphology and edge structures. The results also indicate that control of growth temperature and deposition rate could enable growth of ultrathin borophene ribbons. In addition to elucidating pathways toward improved borophene growth, these findings are likely applicable to the growth of other anisotropic 2D materials.

RESULTS AND DISCUSSION

The growth of 2D structures is energetically determined by the competition between bulk and edge energies. Thus, to elucidate the mechanisms of borophene growth, the structures and energy of

[1]State Key Laboratory of Mechanics and Control of Mechanical Structures, Key Laboratory for Intelligent Nano Materials and Devices of Ministry of Education, and Institute of Nano Science, Nanjing University of Aeronautics and Astronautics, Nanjing 210016, China. [2]Department of Materials Science and NanoEngineering and Department of Chemistry, Rice University, Houston, TX 77005, USA. [3]Center for Nanoscale Materials, Argonne National Laboratory, 9700 South Cass Avenue, Building 440, Argonne, IL 60439, USA. [4]Department of Materials Science and Engineering, Northwestern University, 2220 Campus Drive, Evanston, IL 60208, USA. [5]Applied Physics Graduate Program, Northwestern University, 2220 Campus Drive, Evanston, IL 60208, USA. [6]Department of Chemistry, Northwestern University, 2220 Campus Drive, Evanston, IL 60208, USA.
*Corresponding author. Email: chuwazhang@nuaa.edu.cn (Z.Z.); m-hersam@northwestern.edu (M.C.H.); biy@rice.edu (B.I.Y.)

borophene edges must be determined for the Ag(111) growth substrate. We mainly focus on the $v_{1/6}$ and triangular sheets since they both have been proposed as the atomic models of recently synthesized borophene (*22*, *23*). Different from graphene and h-BN, the two models are strongly anisotropic with four principal edges, two armchair (A_1 and A_2) and two zigzag (Z_1 and Z_2), as illustrated in Fig. 1A and fig. S1.

The most stable structure of each edge is determined by comparing the energy of several enumerated edge structures (figs. S1 and S2). Figure 1B presents the energetically favorable edge structures, which display substantial reconstruction. The lattices at the A_1 and A_2 edges show decreased HH concentration compared to that in the bulk-like region. The two armchair edges are purely flat and weakly interacting with the substrate, indicative of their high chemical stability. Similarly, flat edges are intrinsic to planar boron molecules (*9*, *34*, *35*) and boron sheets with large holes (*36*). Different behavior occurs at the Z_1 and Z_2 edges, which follows a zigzag shape but with a larger periodicity than that defined by the original borophene lattice. The boron atoms at sawtooth tips interact substantially with Ag, while all other edge atoms remain rather inert. The edge reconstruction results from a large variability of boron coordination that enables self-passivation of edge dangling bonds.

We calculate the edge energy using $\gamma = (E_{syst} - E_{sub} - n\mu_B)/2L$, where E_{syst} is the energy of the whole system; E_{sub} and μ_B are the energies of the Ag substrate and chemical potential of boron, respectively; n is the number of boron atoms in the system; and L is the edge length. We adopt μ_B as the energy per atom of a perfect borophene on Ag(111). Because of the reconstructions, the edges have exceptionally small energies on Ag(111), ranging from 0.06 to 0.18 eV/Å, about one-fifth of those for graphene on the same substrate. Note that one cannot exclude even more stable structures for both the Z_1 and Z_2 edges, if larger edge protrusion and longer periodicity are considered (fig. S2); these larger periods are computationally unaffordable but can be the subject of future work. Similar edge reconstructions are also found for the triangular sheet, but the edge energies are notably higher because of the puckered geometry of the sheet (fig. S3).

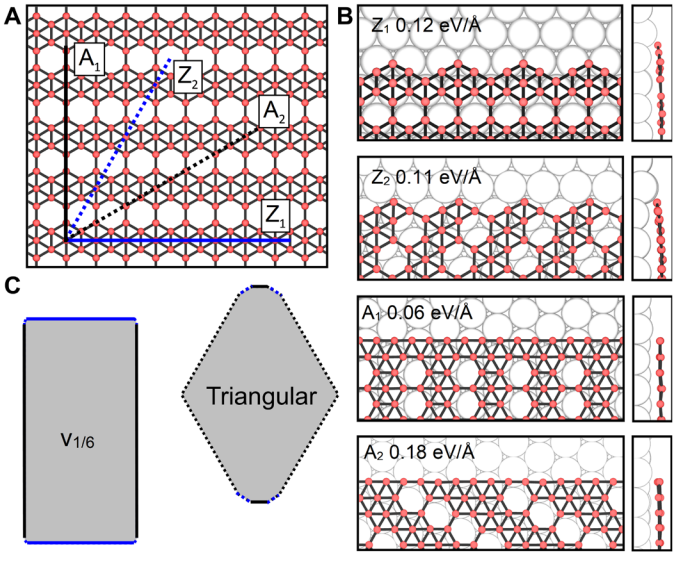

Fig. 1. Borophene edges on silver. (**A**) The $v_{1/6}$ sheet has two armchair edges, denoted as A_1 and A_2, and two zigzag edges, denoted as Z_1 and Z_2. (**B**) Preferred edges of the $v_{1/6}$ sheet on Ag(111) along with calculated edge energies. (**C**) Equilibrium shapes of the $v_{1/6}$ and triangular sheets. Black and blue lines stand for the A_1 and Z_1 edges, while black and blue dotted lines stand for the A_2 and Z_2 edges, respectively.

On the basis of the energy of principal edges, we obtain the edge energy γ for an arbitrary direction χ with respect to the Z_1 direction, through the same analysis developed for graphene. The edge energy γ is expressed as (*37*) $\gamma(\chi) = |\gamma|\cos(\chi + C)$, where $|\gamma| = 2(\gamma_{Ax}^2 + \gamma_{Zx}^2 - \sqrt{3}\gamma_{Ax}\gamma_{Zx})^{1/2}$ and $C = \mathrm{sgn}(\chi)\cdot\arctan(\sqrt{3} - 2\gamma_{Zx}/\gamma_{Ax})$, where γ_{Ux} (U = A and Z; x = 1 and 2) represents the edge energy of the principal edges. The subscripted Ux can be Z_1 and A_2 for $0° < \chi \leq 30°$, Z_2 and A_2 for $30° < \chi \leq 60°$, and Z_2 and A_1 for $60° < \chi \leq 90°$. Then, thermodynamic Wulff construction can determine the equilibrium shape of borophene, the one with the minimal interface energy at a fixed area, by plotting γ versus the edge direction χ, as shown in Fig. 1C for the $v_{1/6}$ and triangular sheets. The equilibrium shape of the $v_{1/6}$ sheet is a rectangle (chopped by ~5% at its corners by the Z_2 edge), while that of the triangular sheet is a rhombus with two sharp corners truncated. Apparently, both shapes do not agree with experimental observations (*22*). However, the equilibrium shape of the $v_{1/6}$ sheet is closer to experiments than that of the triangular sheet. Moreover, a very recent experiment (*27*) has essentially excluded the triangular sheet as the model of synthesized borophenes (*14*). We thus turn to explore the growth kinetics of the $v_{1/6}$ sheet, and further analysis on the triangular sheet is not warranted.

The growth-advancement rate of an entire individual edge depends on the local growth kinetics along the edge. It is thus necessary to calculate the detailed sequence of atom accretion to each edge and then determine the kinetic barrier of growth. To this end, we invoke the idea of step-flow growth of crystals (*38*), which dictates that each edge moves forward by incorporating feeding species to its active sites, manifested as kink flows. Before the incorporation, the feeding species need to find a preferred state and then diffuse on the substrate. We thus compare the energy and dynamics of three candidate species: monomers, dimers, and trimers. The most stable adsorption site is in the subsurface for the three species: the octahedral site for monomers and the inlay interstitial site within the topmost Ag layer for dimers and trimers (fig. S4). The chemical potentials of boron for the three species at their preferred site are −4.18, −4.89, and − 5.19 eV, respectively. The diffusion barriers for monomers and dimers within the subsurface region are 0.26 and 0.59 eV, respectively, indicating their high mobility at experimental growth temperatures of 300° to 700°C. While trimers are more stable than monomers and dimers, trimers also have a significantly higher diffusion barrier. In reality, the entropy contribution at growth conditions further stabilizes monomers and dimers with respect to trimers. The trade-off between stability and mobility renders dimers as the most likely species for feeding growth. We thus take B dimers as the feeding species to compute the growth kinetics of borophene and will consider the effect of monomers later.

First, we add B dimers step by step to the A_1 edge. At each growth step, we scan a number of adsorption sites and determine the optimal configuration by comparing the system energy. However, since the configuration of the nth step has to be built on that of the n − 1th step, the low-energy configuration at a given step may not lead to the optimal EP for the edge growth. The optimal EP must be the one with the overall lowest barrier (mathematically, lowest maximum point), not lowest at every step. This is particularly true for borophene in light of the highly variable coordination of boron that results from the multicenter characteristics of its chemical bonds. Therefore, we

also examine possible branching of the EPs at each step by adding atoms to the second lowest and even third lowest previous configurations. Figure 2 (A and B) depicts the evolution of atomic configurations along the optimal EPs of sequential addition of B dimers to the A_1 and Z_1 edges. At the A_1 edge, the first added dimer is found to pull out a B atom that originally filled an HH at the edge, forming a deformed HH at the kink site. Then, the addition of the second dimer leads to the nucleation of a new row at the edges, which serves as a base for subsequent attachment of B dimers. For the Z_1 edge, the formation of HHs is also energetically preferred during the growth, yet more atoms are needed to nucleate a new row. The growth kinetics at other principal and screwed edges shows similar behavior (figs. S5 to S9). Along the minimum EPs, complete growth of a new row results in a seamless extension of the $v_{1/6}$ lattice while shifting the reconstructed edges along the growth direction by one lattice constant. This structure "replication" is noteworthy in view of the polymorphic nature of borophene that generally allows a diverse arrangement of HHs.

The configurational spectra at each step of growth at the A_1 and Z_1 edges are shown in Fig. 2C. These results further confirm that the configurations that seamlessly extend the borophene lattice are in low-energy regions, while the topological defects and protrusions are in high-energy regions. Consequently, branching into dendrites is unlikely to occur during the borophene growth, consistent with experimental observations. The evolution of free energy during the edge growth also reveals strong kinetic anisotropy. For example, at a boron chemical potential bias of $\Delta\mu = 0.01$ eV near the equilibrium, the kinetic barriers in the optimal EPs are 2.07 and 1.78 eV for the Z_1 and Z_2 edges and decrease to 1.1 and 0.6 eV for the A_1 and A_2 edges, respectively (Fig. 3A). The edge growth proceeds mainly via two steps, row nucleation and kink movement. Both the steps consume more than 10 atoms because of the edge reconstruction and structural anisotropy, in stark contrast to the cases of graphene (*30*) and h-BN (*32*) growths that need only 2 to 3 atoms. Because of the limitation imposed by the used supercell size, the energy profiles do not display the expected periodic up-down levels corresponding to kink flow. However, the energy barriers should be reliable for differentiating growth kinetics across different edges, as the kinetics are determined at the stage of row nucleation that is well accommodated by our supercells.

Different from the linear dependence of equilibrium shapes on the edge energy, the growth rates at the edges depend exponentially on the kinetic barriers, strongly amplifying the anisotropy (*31*). Therefore, all the skewed edges (figs. S7 to S9) and the two armchair edges advance quickly via kink flow. In particular, these edges disappear during growth, as confirmed by the slowest growth of zigzag edges. As a result, a borophene island is terminated only with the Z_1 and Z_2 edges. We first consider the case near thermodynamic equilibrium, where we set the boron chemical potential bias to $\Delta\mu = 0.01$ eV and the growth temperature to $k_BT = 0.08$ eV (~900 K). The kinetic Wulff construction (*30*, *39*) determines the shape of a crystal based on edge growth rates. By modifying the expression of growth velocity versus lattice orientation χ for graphene edges (*30*) to account for lattice anisotropy, we determine the borophene shape to be an

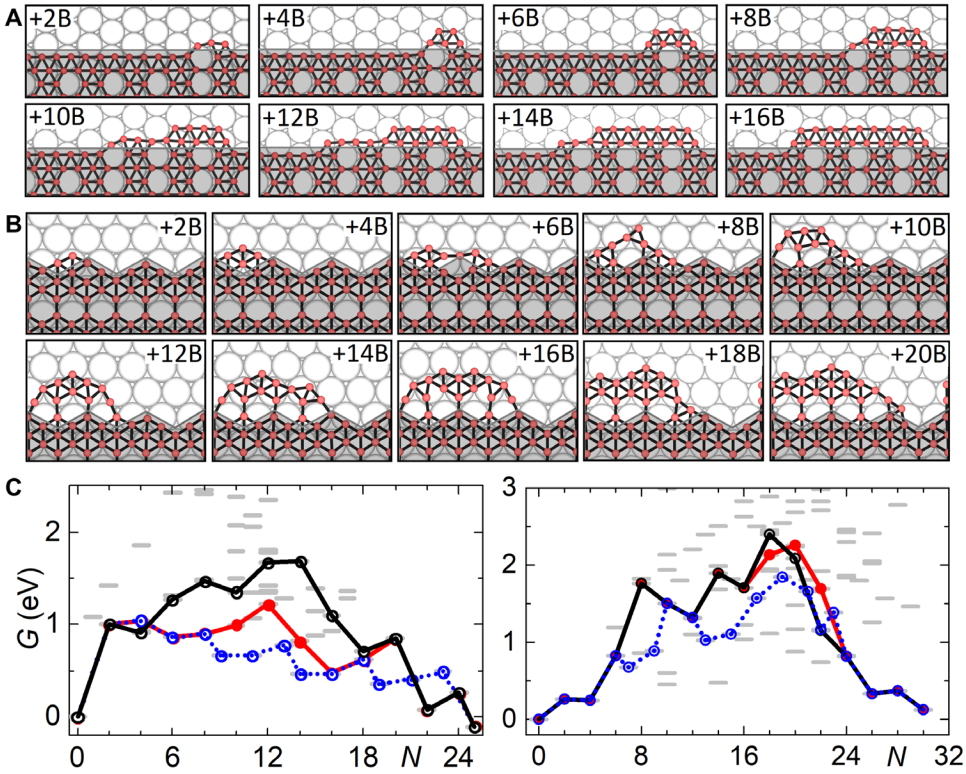

Fig. 2. Growth kinetics of borophene on silver. Energetically optimal atomic configurations during the step-by-step addition of boron dimers to (**A**) A_1 and (**B**) Z_1 edges. (**C**) EPs for the kinetic growth along the (left) A_1 and (right) Z_1 edges, with $\Delta\mu_B = 0$ eV. At each step, we scanned a number of candidate structures whose energies are shown by gray bars. The red solid lines present the optimal EP, while the black solid lines show another EP with a slightly higher maximum. The blue dotted lines show the case of a mixture of monomers and dimers as feeding species.

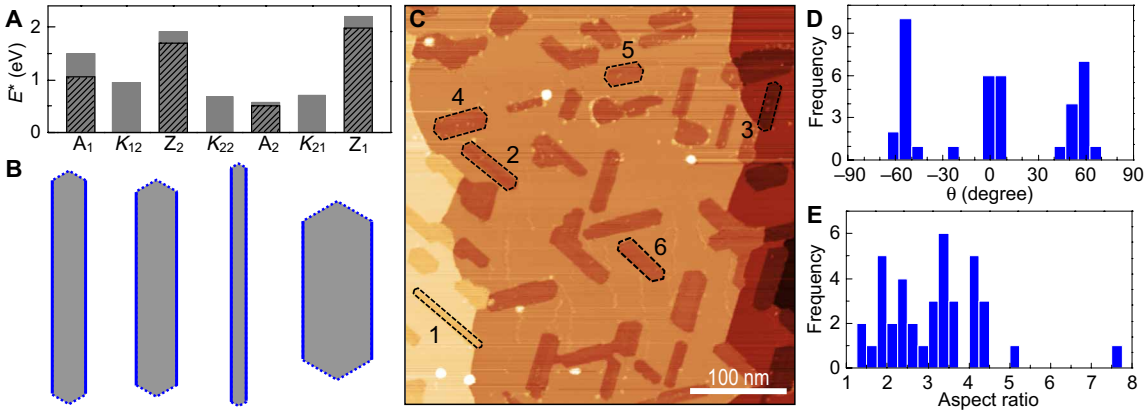

Fig. 3. Kinetic equilibrium shapes of borophene on silver. (**A**) Growth barriers at different edges with $\mu_B = 0.01$ eV. The hatched bars denote energy barriers of the optimal EPs for the growth of different edges, while the shaded bars denote barriers of the EPs shown by the black lines in Fig. 2C. The K_{12}, K_{22}, and K_{21} label the data for the screwed edges illustrated in figs. S7 to S9, respectively. (**B**) Borophene shapes resulting from combinations of growth barriers at different edges shown in (A). The four shapes result from barrier combinations 2.07 eV (Z_1) versus 1.78 eV (Z_2), 2.21 eV (Z_1) versus 1.93 eV (Z_2), 2.07 eV (Z_1) versus 1.93 eV (Z_2), and 2.21 eV (Z_1) versus 1.78 eV, respectively. (**C**) Large-scale scanning tunneling microscopy (STM) topography image of borophene islands ($V_{sample} = 2.0$ V and $I_t = 100$ pA). Typical islands are marked by the numbers 1 to 6. (**D**) Statistics of orientations of borophene islands with respect to Ag(111). (**E**) Statistical distribution of aspect ratios of islands.

elongated hexagon, enclosed by two opposite Z_1 edges and four Z_2 edges in between, as shown by the leftmost image of Fig. 3B, in agreement with the experimental borophene islands shown in Fig. 3C. The elongated hexagon for borophene is unique among 2D materials grown on an isotropic substrate. Increasing the chemical potential of boron and the growth temperature both reduce the kinetic anisotropy of edge growth and shift the shape toward a standard hexagon, as exemplified by the cases of $\Delta\mu = 0.05$ eV at $k_BT = 0.08$ eV and $\Delta\mu = 0.01$ eV at $k_BT = 0.1$ eV (fig. S10).

In addition to the optimal EPs, we also identify alternative EPs for edge growth, which essentially follow the minimum EPs, with deviations arisen mostly in the region around the energy barriers (Figs. 2C and 3A). These EPs give slightly higher growth barriers of 2.21 and 1.93 eV for the Z_1 and Z_2 edges and 1.54 and 0.68 eV for the A_1 and A_2 edges, respectively, at $\Delta\mu = 0.01$ eV. We anticipate additional EPs with different barriers, but these EPs cannot be fully calculated because of prohibitively high computational cost imposed by the large-scale atomic models. Regardless, the additional computationally accessible EPs confirm the anisotropy of edge growth, but they mediate the competition between growth of Z_1 and Z_2 edges, ultimately leading to diversity of shapes. As seen in Fig. 3B, the shapes resulting from combinatorics of different barriers at Z_1 and Z_2 edges remain elongated hexagons yet show different aspect ratios. It is encouraging that these hexagons reproduce the experimentally observed shapes of borophene well, as marked by numbers 1 to 6 in Fig. 3C. Of particular interest are the needle-like ribbon structures that result from the combination of $E_{Z1} = 2.21$ eV and $E_{Z2} = 1.78$ eV, which can potentially function as a conductive wire of atomic width for nanoelectronic devices. According to our theory, lowering the growth temperature and chemical potential of boron can enhance the kinetic anisotropy in a manner that will promote the growth of ultranarrow boron nanoribbons. In Fig. 3C, we find that the needle-like islands tend to appear separately from other islands (labeled by number 1), which, to some extent, supports our theory in a sense that the supply of boron for growing the narrow ribbons should be locally limited.

Our experimental islands show additional interesting points. First, as a result of the sixfold symmetry of the Ag(111) surface, the islands are oriented with an expected three-peak distribution (i.e., at −60°, 0°, and 60°; see Fig. 3D), indicating that these islands share the same registry with the substrate, as adopted in our models. Second, a statistical analysis of the island aspect ratios, shown in Fig. 3E, suggests that the shapes are skewed toward elongation. The islands of the highest frequency have an aspect ratio of ~3.5, which agrees well with the value (~4) determined by the optimal EPs at $\Delta\mu = 0.01$ eV and $k_BT = 0.08$ eV. Despite the scattered distribution of aspect ratios, the island areas are relatively centered at ~450 nm^2, which indicates a possible anticorrelation of the growth at the Z_1 and Z_2 edges; namely, rapid growth of one edge retards growth of the other while keeping the overall growth rate of an island unchanged. The aspect ratio of a specific island thus depends on the relative orientation between the edges and flow of deposited feeding species as well as the local nucleation density.

If boron were provided in the form of mixed monomers and dimers, then the accretion sequence possibilities would be more broadened. One benefit is that some high-energy states during the edge growth can be skipped, resulting in an EP with a lower kinetic barrier for each edge (Fig. 2C). As a result, the growth can be faster and perhaps have higher quality than that with dimers alone. The corresponding barriers for the Z_1 and Z_2 edges are reduced to 1.84 and 1.2 eV, respectively, shaping the borophene island into an elongated hexagon with an increased aspect ratio (more ribbonlike; fig. S11). In any case, it is clear that the anisotropic growth kinetics of borophene are rather robust against the variation of feeding species.

While the borophene shapes have been well described by the growth kinetics, it is important to see whether the lattice structure and edge orientation of borophene islands also match the models. To this end, we examine the scanning tunneling microscopy (STM) image of a typical island with an elongated hexagonal shape (Fig. 4A). Atomically resolved images reveal an island in the striped phase reported in a previous work (*22*), with a rectangular unit cell (Fig. 4A, inset). A comparison of experimental and simulated STM topography images (Fig. 4, A and B) confirms that the $v_{1/6}$ sheet matches key features of the island, especially the lattice constant and the striped pattern. This comparison enables us to deduce that the long edge of the island is oriented along the HH rows, i.e., the direction of the Z_1 edge in our model (Fig. 4B), and the four short edges are oriented along the Z_2 edge. Moreover, the measured lattice periodicity based on the derivative of the STM topography is

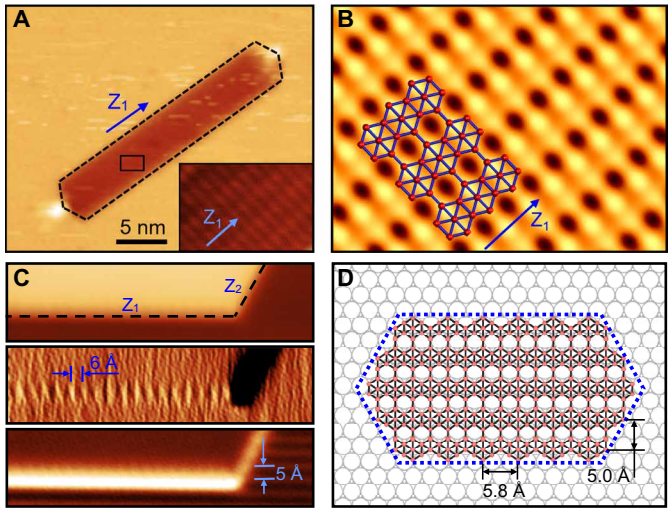

Fig. 4. Edges and lattices of borophene islands. (**A**) STM topography image of a borophene island (V_{sample} = 0.1 V and I_t = 1.0 nA). Inset: Zoomed-in image of the area marked by the black rectangle. (**B**) Simulated STM image of the $v_{1/6}$ sheet on silver, overlaid with an atomic model (V_{sample} = 1.0 V). The blue arrow indicates the Z_1 direction. (**C**) Top: STM topography image of the Z_1 and Z_2 edges of a typical borophene island (V_{sample} = 2.0 V and I_t = 100 pA). The lattice periodicities of the two edges are measured by *x* (middle) and *y* (bottom) derivatives of the STM topography. (**D**) Schematic model of a $v_{1/6}$ sheet island on Ag(111) along with calculated edge periodicities.

0.6 Å for the Z_1 edge (Fig. 4C), again in agreement with the value of 0.58 Å predicted by the theoretical model (Fig. 4D). Similar agreement between theory and experiment is also obtained for the Z_2 edge.

CONCLUSIONS

On the basis of ab initio calculations and experimental characterization, we have identified the edges of borophene on silver and elucidated the growth mechanism including the island shape and morphology of the edges. Borophene is revealed to have significant edge reconstructions that result in low edge energy and doubled periodicities of its intrinsic lattice. The thermodynamic equilibrium shape is predicted to be approximately rectangular yet is absent in experimental observation. However, away from equilibrium, we determine the sequence of atomic row assembly at the edges, which not only moves the edges along the growth direction but also seamlessly extends the original borophene lattice. The growth kinetics follow multiple EPs with close barriers along each edge but with strong anisotropy across different edges. Consequently, the kinetic equilibrium shapes of borophene turn out to be a series of elongated hexagons that reproduce the shapes observed experimentally. We further show that the condition of low growth temperature and low boron chemical potential is likely to enable selective growth of ultrathin boron nanoribbons. Overall, these results provide the first atomistic understanding for the growth of borophene, which is likely to inform the high-quality synthesis of other highly anisotropic 2D materials.

MATERIALS AND METHODS

Theory and models

Our model systems consist of borophene nanostructures overlaid on Ag(111) of three atomic layers. The calculations were performed within the framework of density functional theory using a projector augmented wave method for the potential at the core region and generalized gradient approximation of the Perdew-Burke-Ernzerhof functional as implemented in the Vienna Ab initio Simulation Package code (*40*). We adopt a kinetic energy cutoff of 400 eV for the plane-wave expansion and set the vacuum region to 15 Å to isolate neighboring periodic images. The Brillouin zone was sampled at the Γ point only. Borophene nanoribbons were overlaid on Ag(111) to calculate energies of edges and of atom accretion therein. For the latter, the atoms at the nongrowth edge of nanoribbons were fixed to the relaxed positions before growth. The positions of other boron atoms plus metal atoms of the top two layers were relaxed using the conjugate gradient method until the force on each atom was less than 0.01 eV/Å.

Growth and STM of borophene

Borophene samples were grown on Ag(111) single-crystal substrates (99.999%, <0.01° miscut; MaTecK) by electron beam evaporation of a boron rod (99.9999%; ESPI Metals) under ultrahigh vacuum. The substrate was prepared by cycles of Ar ion sputtering and annealing to 550°C. Samples were grown at 550°C, at a boron flux of ~0.05 monolayers/min. After growth, samples were cooled quickly to room temperature by immediate heater shutoff and placement of the sample on a room temperature heat sink. STM images were acquired in Omicron STM/atomic force microscopy systems, at temperatures of 55 and 4 K, respectively, using electrochemically etched W tips.

SUPPLEMENTARY MATERIALS

Supplementary material for this article is available at http://advances.sciencemag.org/cgi/content/full/5/9/eaax0246/DC1

Fig. S1. Considered candidate structures for the Z_1 edge on Ag(111) and their edge energies (eV/Å).
Fig. S2. Considered candidate structures for the Z_2 edge on Ag(111) and their edge energies (eV/Å).
Fig. S3. Preferred edges of the triangular sheet on Ag(111), along with calculated edge energies.
Fig. S4. Energetically preferred atomic configurations for a boron (left) monomer, (middle) dimer, and (left) trimer on Ag(111).
Fig. S5. Growth kinetics at the A_2 edge.
Fig. S6. Growth kinetics at the Z_2 edge.
Fig. S7. Growth kinetics at the K_{12} edge.
Fig. S8. Growth kinetics at the K_{22} edge.
Fig. S9. Growth kinetics at the K_{21} edge.
Fig. S10. Borophene shapes of kinetic equilibrium under other growth conditions.
Fig. S11. Borophene shape of kinetic equilibrium when feeding boron species are provided in the form of mixed monomers and dimers, with $\Delta\mu$ = 0.01 eV and k_BT = 0.08.

REFERENCES AND NOTES

1. Z. Zhang, E. S. Penev, B. I. Yakobson, Two-dimensional boron: Structures, properties and applications. *Chem. Soc. Rev.* **46**, 6746–6763 (2017).
2. A. J. Mannix, Z. Zhang, N. P. Guisinger, B. I. Yakobson, M. C. Hersam, Borophene as a prototype for synthetic 2D materials development. *Nat. Nanotechnol.* **13**, 444–450 (2018).
3. Z. Zhang, E. S. Penev, B. I. Yakobson, Polyphony in B flat. *Nat. Chem.* **8**, 525 (2016).
4. X. Liu, Z. Wei, I. Balla, A. J. Mannix, N. P. Guisinger, E. Luijten, M. C. Hersam, Self-assembly of electronically abrupt borophene/organic lateral heterostructures. *Sci. Adv.* **3**, e1602356 (2017).
5. N. Gonzalez Szwacki, A. Sadrzadeh, B. I. Yakobson, B_{80} fullerene: An *ab initio* prediction of geometry, stability, and electronic structure. *Phys. Rev. Lett.* **98**, 166804 (2007).
6. H. Tang, S. Ismail-Beigi, Novel precursors for boron nanotubes: The competition of two-center and three-center bonding in boron sheets. *Phys. Rev. Lett.* **99**, 115501 (2007).
7. X. Yang, Y. Ding, J. Ni, *Ab initio* prediction of stable boron sheets and boron nanotubes: Structure, stability, and electronic properties. *Phys. Rev. B* **77**, 041402 (2008).
8. A. K. Singh, A. Sadrzadeh, B. I. Yakobson, Probing properties of boron α-tubes by *ab initio* calculations. *Nano Lett.* **8**, 1314 (2008).
9. Z. A. Piazza, H.-S. Hu, W.-L. Li, Y.-F. Zhao, J. Li, L.-S. Wang, Planar hexagonal B_{36} as a potential basis for extended single-atom layer boron sheets. *Nat. Commun.* **5**, 3113 (2014).

10. W.-L. Li, Q. Chen, W.-J. Tian, H. Bai, Y.-F. Zhao, H.-S. Hu, J. Li, H.-J. Zhai, S.-D. Li, L.-S. Wang, The B_{35} cluster with a double-hexagonal vacancy: A new and more flexible structural motif for borophene. *J. Am. Chem. Soc.* **136**, 12257 (2014).
11. H. Tang, S. Ismail-Beigi, Self-doping in boron sheets from first principles: A route to structural design of metal boride nanostructures. *Phys. Rev. B* **80**, 134113 (2009).
12. E. S. Penev, S. Bhowmick, A. Sadrzadeh, B. I. Yakobson, Polymorphism of two-dimensional boron. *Nano Lett.* **12**, 2441–2445 (2012).
13. X. Wu, J. Dai, Y. Zhao, Z. Zhuo, J. Yang, X. C. Zeng, Two-dimensional boron monolayer sheets. *ACS Nano* **6**, 7443–7453 (2012).
14. Z. Zhang, Y. Yang, G. Gao, B. I. Yakobson, Two-dimensional boron monolayers mediated by metal substrates. *Angew. Chem. Int. Ed.* **54**, 13022–13026 (2015).
15. Y. Liu, E. S. Penev, B. I. Yakobson, Probing the synthesis of two-dimensional boron by first-principles computations. *Angew. Chem. Int. Ed.* **52**, 3156–3159 (2013).
16. Z. Zhang, S. N. Shirodkar, Y. Yang, B. I. Yakobson, Gate-voltage control of borophene structure formation. *Angew. Chem. Int. Ed.* **56**, 15421–15426 (2017).
17. E. S. Penev, A. Kutana, B. I. Yakobson, Can two-dimensional boron superconduct? *Nano Lett.* **16**, 2522–2526 (2016).
18. Y. Zhao, S. Zeng, J. Ni, Phonon-mediated superconductivity in borophenes. *Appl. Phys. Lett.* **108**, 242601 (2016).
19. B. Feng, O. Sugino, R.-Y. Liu, J. Zhang, R. Yukawa, M. Kawamura, T. Iimori, H. Kim, Y. Hasegawa, H. Li, L. Chen, K. Wu, H. Kumigashira, F. Komori, T.-C. Chiang, S. Meng, I. Matsuda, Dirac fermions in borophene. *Phys. Rev. Lett.* **118**, 096401 (2017).
20. S. Gupta, A. Kutana, B. I. Yakobson, Dirac cones and nodal line in borophene. *J. Phys. Chem. Lett.* **9**, 2757–2757 (2018).
21. Y. Huang, S. N. Shirodkar, B. I. Yakobson, Two-dimensional boron polymorphs for visible range plasmonics: A first-principles exploration. *J. Am. Chem. Soc.* **139**, 17181 (2017).
22. A. J. Mannix, X.-F. Zhou, B. Kiraly, J. D. Wood, D. Alducin, B. D. Myers, X. Liu, B. L. Fisher, U. Santiago, J. R. Guest, M. J. Yacaman, A. Ponce, A. R. Oganov, M. C. Hersam, N. P. Guisinger, Synthesis of borophenes: Anisotropic, two-dimensional boron polymorphs. *Science* **350**, 1513 (2015).
23. B. Feng, J. Zhang, Q. Zhong, W. Li, S. Li, H. Li, P. Cheng, S. Meng, L. Chen, K. Wu, Experimental realization of two-dimensional boron sheets. *Nat. Chem.* **8**, 563–568 (2016).
24. Q. Zhong, J. Zhang, P. Cheng, B. Feng, W. Li, S. Sheng, H. Li, S. Meng, L. Chen, K. Wu, Metastable phases of 2D boron sheets on Ag(111). *J. Phys. Condens. Matter* **29**, 095002 (2017).
25. W. Li, L. Kong, C. Chen, J. Gou, S. Sheng, W. Zhang, H. Li, L. Chan, P. Cheng, K. Wu, Experimental realization of honeycomb borophene. *Sci. Bull.* **63**, 282–286 (2018).
26. Z. Zhang, A. J. Mannix, Z. Hu, B. Kiraly, N. P. Guisinger, M. C. Hersan, B. I. Yakobson, Substrate-induced nanoscale undulations of borophene on silver. *Nano Lett.* **16**, 6622–6627 (2016).
27. X. Liu, L. Wang, S. Li, M. S. Rahn, B. I. Yakobson, M. C. Hersam, Geometric imaging of borophene polymorphs with functionalized probes. *Nat. Commun.* **10**, 1642 (2019).
28. X. Liu, Z. Zhang, L. Wang, B. I. Yakobson, M. C. Hersam, Intermixing and periodic self-assembly of borophene line defects. *Nat. Mater.* **17**, 783–788 (2018).
29. Q. Zhong, L. Kong, J. Gou, W. Li, S. Sheng, S. Yang, P. Cheng, H. Li, K. Wu, L. Chen, Synthesis of borophene nanoribbons on Ag(110) surface. *Phys. Rev. Mater.* **1**, 021001 (2017).
30. V. I. Artyukhov, Y. Liu, B. I. Yakobson, Equilibrium at the edge and atomistic mechanisms of graphene growth. *Proc. Natl. Acad. Sci. U.S.A.* **109**, 15136–15140 (2012).
31. V. I. Artyukhov, Y. Hao, R. S. Ruoff, B. I. Yakobson, Breaking of symmetry in graphene growth on metal substrates. *Phys. Rev. Lett.* **114**, 115502 (2015).
32. Z. Zhang, Y. Liu, Y. Yang, B. I. Yakobson, Growth mechanism and morphology of hexagonal boron nitride. *Nano Lett.* **16**, 1398–1403 (2016).
33. V. I. Artyukhov, Z. Hu, Z. Zhang, B. I. Yakobson, Topochemistry of bowtie- and star-shaped metal dichalcogenide nanoisland formation. *Nano Lett.* **16**, 3696–3702 (2016).
34. A. P. Sergeeva, I. A. Popov, Z. A. Piazza, W.-L. Li, C. Romanescu, L.-S. Wang, A. I. Boldyrev, Understanding boron through size-selected clusters: Structure, chemical bonding, and fluxionality. *Acc. Chem. Res.* **47**, 1349–1358 (2014).
35. B. Kiran, S. Bulusu, H.-J. Zhai, S. Yoo, X. C. Zeng, L.-S. Wang, Planar-to-tubular structural transition in boron clusters: B_{20} as the embryo of single-walled boron nanotubes. *Proc. Natl. Acad. Sci. U.S.A.* **102**, 961–964 (2005).
36. E. S. Penev, V. I. Artyukhov, F. Ding, B. I. Yakobson, Unfolding the fullerene: Nanotubes, graphene and poly-elemental varieties by simulations. *Adv. Mater.* **24**, 4956–4976 (2012).
37. Y. Liu, A. Dobrinsky, B. I. Yakobson, Graphene edge from armchair to zigzag: The origins of nanotube chirality? *Phys. Rev. Lett.* **105**, 235502 (2010).
38. W. K. Burton, N. Cabrera, F. C. Frank, The growth of crystals and the equilibrium structure of their surfaces. *Philos. Trans. R. Soc. Lond. A* **243**, 299–358 (1951).
39. R. F. Sekerka, Equilibrium and growth shapes of crystals: how do they differ and why should we care? *Cryst. Res. Technol.* **40**, 291–306 (2005).
40. G. Kresse, J. Hafner, *Ab initio* molecular-dynamics simulation of the liquid-metal–amorphous-semiconductor transition in germanium. *Phys. Rev. B* **49**, 14251 (1994).

Acknowledgments

Funding: Work at NUAA was supported by the National Natural Science Foundation of China (11772153) and the Research Fund of State Key Laboratory of Mechanics and Control of Mechanical Structures (MCMS-0417G01, NE2018002). Work at Rice University was supported by the Department of Energy BES grant DE-SC0012547. Support from the Office of Naval Research (ONR N00014-17-1-2993) and the NSF Materials Research Science and Engineering Center (NSF DMR-1720139) is also acknowledged. This work was performed, in part, at the Center for Nanoscale Materials, a U.S. Department of Energy Office of Science User Facility, and supported by the U.S. Department of Energy, Office of Science, under contract no. DE-AC02-06CH11357. **Author contributions:** Z.Z. conceived the idea and performed the calculations. A.J.M. and X.L. performed the experiments. B.I.Y., M.C.H., and N.P.G. supervised the research. Z.H. helped with the data analysis. Z.Z., B.I.Y., and M.C.H. wrote the paper. All the authors discussed the results and commented on the manuscript. **Competing interests:** The authors declare that they have no competing interests. **Data and materials availability:** All data needed to evaluate the conclusions in the paper are present in the paper and/or the Supplementary Materials. Additional data related to this paper may be requested from the authors.

Submitted 15 February 2019
Accepted 29 August 2019
Published 27 September 2019
10.1126/sciadv.aax0246

Citation: Z. Zhang, A. J. Mannix, X. Liu, Z. Hu, N. P. Guisinger, M. C. Hersam, B. I. Yakobson, Near-equilibrium growth from borophene edges on silver. *Sci. Adv.* **5**, eaax0246 (2019).

Science Advances

Near-equilibrium growth from borophene edges on silver

Zhuhua Zhang, Andrew J. Mannix, Xiaolong Liu, Zhili Hu, Nathan P. Guisinger, Mark C. Hersam and Boris I. Yakobson

Sci Adv **5** (9), eaax0246.
DOI: 10.1126/sciadv.aax0246